

Dalton Transactions

Accepted Manuscript



This is an *Accepted Manuscript*, which has been through the Royal Society of Chemistry peer review process and has been accepted for publication.

Accepted Manuscripts are published online shortly after acceptance, before technical editing, formatting and proof reading. Using this free service, authors can make their results available to the community, in citable form, before we publish the edited article. We will replace this *Accepted Manuscript* with the edited and formatted *Advance Article* as soon as it is available.

You can find more information about *Accepted Manuscripts* in the [Information for Authors](#).

Please note that technical editing may introduce minor changes to the text and/or graphics, which may alter content. The journal's standard [Terms & Conditions](#) and the [Ethical guidelines](#) still apply. In no event shall the Royal Society of Chemistry be held responsible for any errors or omissions in this *Accepted Manuscript* or any consequences arising from the use of any information it contains.

Effect of local A-site strain on dipole stability in $A_6\text{GaNb}_9\text{O}_{30}$ (A = Ba, Sr, Ca) tetragonal tungsten bronze relaxor dielectrics

Andrew J. Miller¹, Andrei Rotaru^{1,2,3}, Donna C. Arnold^{1,4}, Finlay D. Morrison^{1,*}

¹EaStCHEM School of Chemistry, University of St Andrews, North Haugh, St Andrews, Fife KY16 9ST, UK.

²University of Craiova, Faculty of Mathematics and Natural Sciences, A.I. Cuza Str, Nr. 13, Craiova, Romania

³INFLPR – National Institute for Laser, Plasma and Radiation Physics, Laser Department, Bvd. Atomistilor, Nr. 409, RO-077125 Magurele (Jud. Ilfov), Bucharest, Romania.

⁴School of Physical Sciences, University of Kent, Canterbury, CT2 7NH, UK.

Abstract

A series of isovalently A-site substituted relaxor dielectric tetragonal tungsten bronzes of general formula $\text{Ba}_{6-x-y}\text{Sr}_x\text{Ca}_y\text{GaNb}_9\text{O}_{30}$ were investigated. The long-range (average) crystal structure as determined by conventional diffraction techniques varies monotonically according to Vegard's law. The dielectric properties, however, do not display a similar, simple "average size" dependence and instead show a dependence on the statistical size variance, *i.e.* size mismatch, of the A-cation. The difficulties in Vogel-Fulcher analysis of relative permittivity and the complementary approach of using dielectric loss data fitted to Jonscher's empirical Universal Dielectric Relaxation model is discussed.

Introduction

The tetragonal tungsten bronze (TTB) structure, general formula $\text{A}_1\text{A}_2\text{A}_4\text{B}_1\text{B}_2\text{B}_8\text{C}_4\text{X}_{30}$, is closely related to perovskite ABX_3 in that it consists of a 3-dimensional corner sharing network of BX_6 octahedra^{1,2}. An alternative description is that TTBS consist of "columns" of perovskite (formed by $\text{A}_1\text{B}_2\text{X}_3$ units) running along the short *c*-axis and which are interconnected by additional

B1X₆ octahedra. The result is the formation of an additional, large 15 coordinate A2-site and a smaller 9 coordinate C-site. The TTB aristotype structure (space group *P4/mbm*, No. 127) is shown in Figure 1 (a). In general, the same elements occupy the A, B and X sites in both perovskite and TTBs, although the A2 site is slightly more limited to larger cations; the C-site is generally only occupied by Li⁺. TTBs offer a wider compositional flexibility than perovskites not only due to the presence of more crystallographically distinct cation sites, but also due to their ability to have highly variable stoichiometry: so-called “stuffed” TTBs have all 5 cation sites fully occupied; filled TTBs have full occupancy of the A- and B-sites while the C-sites are vacant; unfilled TTBs typically have only 5/6 occupancy of the A-sites, while the B- and C-sites are full and empty, respectively. As a result, TTBs display a wide range of properties, but they have been most widely studied in the context of dielectric and ferroelectric oxides such as Ba₂NaNb₅O₁₅ (BNN)^{3, 4}, (Sr,Ba)Nb₂O₆ (SBN)⁵, and the family Ba₂RTi₂Nb₃O₁₅ (RE = La, Nd, Sm, Gd, Dy and Bi)^{6, 7}.

Recently we reported on a family of filled TTBs of general formula Ba₆MNb₉O₃₀ (M³⁺ = Fe, Ga, Sc, In and Y)⁸⁻¹⁰ which display relaxor behaviour in their dielectric response, *i.e.*, a frequency dispersion in both the real and imaginary components of the complex permittivity. We observed that in these materials the dipole stability (characterised by the temperature of the peak in the permittivity) increases as the size of the M³⁺ cation increases and this results from an increase in the tetragonality (*c/a*) which allows increased dipolar displacements of the B-cations along the *c*-axis⁹. We also showed that this correlation of dielectric response and tetragonality could be extended to other filled TTBs, and could also be used as a simplified approximation in more complex unfilled TTB compositional series¹¹. However, specifically for the Ba₆MNb₉O₃₀ (M³⁺ = Ga, Sc, In) series we used a combination of temperature dependent, high resolution powder neutron diffraction and in-depth electrical characterisation to show that these materials more closely resemble dipole glass relaxors rather than relaxor ferroelectrics in nature and that the dipolar response predominantly originates from B1 displacements along the *c*-axis; a simple mechanism whereby the *c*-axis is extended by inclusion of larger B-cations allowing larger and more stable displacements explains the observed change in dielectric properties – a simple B-cation size effect⁹.

In this article we describe some aspects of our investigation into the effect of varying A-cation size in this structural family by systematically replacing Ba^{2+} in $\text{Ba}_6\text{GaNb}_9\text{O}_{30}$ by the smaller Sr^{2+} and Ca^{2+} cations at the A-site. We show that a simple “average size” effect cannot be extended to this family and that instead local strain variations due to the cation size mismatch (quantified by statistical size variance) is more successful. In this respect, “average” crystal structure data obtained from traditional powder diffraction methods is not sensitive to such local variations and we show how in-depth analysis of dielectric data can be a useful tool, and also highlight some of the pit-falls and problems associated with such analysis.

Experimental

Materials with the general formula $\text{Ba}_{6-x-y}\text{Ca}_x\text{Sr}_y\text{GaNb}_9\text{O}_{30}$ were prepared from BaCO_3 , SrCO_3 , CaCO_3 , Ga_2O_3 and Nb_2O_5 (all Aldrich, 99+ %) using standard solid-state methods as described elsewhere⁸. Stoichiometric ratios of the starting materials were ball milled and subjected to the following heating regime; 4 hours at 1000 °C, 10 hours at 1250 °C and 6 hours at 1300 °C. Phase formation was confirmed by powder x-ray diffraction (XRD) collected in transmission mode using a STOE diffractometer equipped with $\text{Cu K}\alpha_1$ radiation (40 kV and 30 mA, $\lambda = 1.54413 \text{ \AA}$) over a range of $20 \leq 2\theta \leq 60$. Powder neutron diffraction (PND) measurements were conducted at a constant wavelength ($\lambda = 1.5943201 \text{ \AA}$) on the D2b beamline at the Institut Laue-Langevin (ILL). Neutron data were collected at room temperature with the materials loaded into 8 mm cylindrical vanadium cans. Pellets were prepared for electrical characterisation at 1300 °C and all exhibited > 90 % theoretical density. Pt electrodes were applied using Pt paste (Gwent Electronic Materials Ltd.) and cured at 900 °C for approximately 20 minutes. Dielectric measurements were made using a Agilent 4294A impedance analyser over a frequency range of 10 Hz – 13 MHz and a temperature range of approximately 20 – 340 K in a Sumitomo closed-cycle He cryocooler.

Results

Effect of average A-cation size: $\text{Ba}_{6-x-y}\text{Sr}_x\text{Ca}_y\text{GaNb}_9\text{O}_{30}$

XRD confirmed a significant phase field for formation of the TTB phase, extending to $x = 4.5$ in the case of Sr-substitution and $y = 3$ for Ca and $x = 1$, $y = 2$ and $x = 3$, $y = 2$ for co-doped compositions, Figure 1 (b). Room temperature lattice parameters were obtained by Rietveld refinement of PND data in the centrosymmetric space group $P4/mbm$. Full details of the refinements and refinement data are presented in the ESI. All compounds followed Vegard's law with a systematic decrease in both the ab and c directions, and hence volume, with decreasing average A-cation size, $\langle r_A \rangle$, Figure 2. (Calculations were based on 12 co-ordinate data obtained from Shannon¹²: $r_{Ba} = 1.61 \text{ \AA}$, $r_{Sr} = 1.44 \text{ \AA}$ and $r_{Ca} = 1.36 \text{ \AA}$).

Dielectric data showed that all compositions exhibited relaxor-like behaviour with a similar degree of frequency dispersion in the permittivity-temperature profile. Both Sr-, Ca- and Sr+Ca co-doping resulted in a displacement of the temperature of the peak maximum (T_m) in the permittivity from that observed for the $Ba_6GaNb_9O_{30}$ parent compound. The loss peaks were also similarly displaced. However the change in T_m does not correlate systematically with the observed changes in the unit cell parameters, *i.e.*, $\langle r_A \rangle$, Figure 3 (a), and hence the expected change in tetragonality as observed for the B-site substituted compounds. (The isotropic contraction with decreasing average A-cation size means that the tetragonality also decreases monotonically with decreasing $\langle r_A \rangle$). Instead T_m appears to vary systematically with the statistical A-cation size variance, σ^2 where:

$$\sigma^2 = \langle r_A^2 \rangle - \langle r_A \rangle^2 \quad (1)$$

where r_A is the ionic radius of the cation at the A-site. Here σ^2 simply describes the relative size distribution of cations occupying the A-site¹³. Whereas diffraction averages out any A-cation size differences giving a time and spatially averaged picture of the unit cell dimensions, the variance gives a quantitative measure of the degree of local disruption to be expected and hence magnitude of the "local strain" experienced by the lattice around the dopant cation point defects. First introduced by Attfield *et al.*¹³, the size variance has been successfully used to explain the temperature dependence of magnetic phase transition in perovskite manganites and subsequently the unusual change in the ferroelectric Curie temperature in Ca-doped $BaTiO_3$ ¹⁴. It is clear that there is also a correlation with local effects (quantified by σ^2) and dipole stability in these materials, Figure 3 (b). If the PND data gives the "average change" in crystal structure and σ^2

allows some metric of local change then for the data in Figure 4 (b), both the “local” (variance) and “average” (unit cell) structure is changing - the key experiment was therefore to decouple the two.

Varying “local” vs. constant “average” structure

In order to decouple the two effects we adopted the approach used by Sinclair and Attfield¹⁴: starting from the Sr-doped composition $\text{Ba}_4\text{Sr}_2\text{GaNb}_9\text{O}_{30}$ we systematically replaced the Sr with the appropriate ratio of larger Ba^{2+} and smaller Ca^{2+} ions such that their average size is equivalent to Sr being replaced: $r_{\text{Sr}} = 0.37r_{\text{Ba}} + 0.63r_{\text{Ca}} = 1.44 \text{ \AA}$. This doping mechanism can be described by the general formula $\text{Ba}_4\text{Sr}_{2-z}(\text{Ba}_{0.37}\text{Ca}_{0.63})_z\text{GaNb}_9\text{O}_{30}$ and allows a series of compositions to be prepared with a constant overall $\langle r_A \rangle = 1.55 \text{ \AA}$, but with varying size variance, σ^2 . Four TTB compositions with $z = 0.5, 1.0, 1.5$ and 2.0 were prepared and their XRD patterns are shown in Figure 4. All adopt the $P4/mbm$ TTB structure and basic Rietveld refinements (including only background, zero point and unit cell) were carried out to obtain lattice parameters. The data showed that, as expected, the long-range, average structure (and tetragonality) is essentially unchanged but the variance varies significantly with z , Table 1. Dielectric data indicated that all compositions exhibit relaxor behaviour, Figure 5, and the dielectric curves displaced to higher temperature with increasing z (see ESI). In order to more closely quantify the changes in dielectric response we used the most common approach of fitting the frequency dependence of the temperature of the permittivity maximum, T_m according to the Vogel-Fulcher (VF) expression¹⁵:

$$f = f_0 \exp\left(-\frac{E_A}{k(T_m - T_f)}\right) \quad (2)$$

where f is the frequency of applied field, f_0 is the fundamental dipole (attempt) frequency for polarisation perturbation, E_A is the activation energy associated with dipole realignment and T_f is the dipole freezing temperature. While T_m can arguably be used as a first approximation of dipole stability, and can be used for comparison among materials with similar degrees of frequency dispersion, T_f provides an “intrinsic” frequency independent parameter. Initially data were fitted with all three fitting parameters (f_0 , E_A and T_f) unconstrained and the results presented in Table 2.

The goodness-of-fit parameters suggest the VF model is a good representation of the dielectric response, with the fits shown in Figure 6, however, there was no systematic trend in T_f or E_A with z ; the values of f_0 vary far more widely than would be expected for such a structurally similar series and, more importantly, in some cases are physically unrealistic for the process they describe (dipolar relaxation frequencies should be of the order 10^9 - 10^{12} Hz).

The uncertainty over the reliability of the values calculated from the unconstrained VF fits suggested that it might be desirable to re-fit the curves using a restricted, and physically realistic, value for f_0 . The unconstrained fit to the data for the $x = 0.5$ sample gave a physically realistic value for f_0 of 8.42×10^{11} Hz and this was constrained as the value in subsequent fits for the other three compositions. Visually there was no apparent deterioration of these ‘constrained’ fits but predictably they did not have such low error analyses (Table 2) as the unconstrained fits. However, they did give physically realistic values for both E_A and T_f for all samples: the values for E_A were within those expected for dipolar processes (of the order of 0.1 eV) and the values of T_f increased systematically with increasing x – as was the expectation from visual inspection of the VF curves, Figure 6. We have previously discussed the inherent sensitivity of VF fits to minor scatter in data points¹⁶ and given that the chosen f_0 value was rather arbitrary (being merely the first realistic value obtained by the unconstrained fit method) this outcome was rather unsatisfying.

As an alternative we analysed the dielectric loss data according to Jonscher’s Universal Dielectric Relaxation (UDR) model¹⁷ to determine E_A and T_f . We have already shown this to be an effective methodology for modelling dielectric relaxation in these materials⁹ – the parameters obtained can then be fed back into the VF analysis in order to further investigate the suitability of the VF fitting process. According to the UDR model the temperature dependence of the peak frequency, f_p in the dielectric loss, Figure 5 (b), should follow an Arrhenius expression:

$$f_p = A \exp\left(-\frac{E_A}{kT}\right) \quad (3)$$

and allows an alternative method to obtain E_A . Arrhenius plots of the loss data for all four samples are given in Figure 7. In each case the data give a straight line, and activation energies

calculated from a line of best fit give E_A values of 0.077, 0.139, 0.159 and 0.253 eV for $z = 0.5$, 1.0, 1.5, and 2.0, respectively (Table 2). These values are all of the expected magnitude for a dipole relaxation process (as for the VF analysis), however, they show a systematic increase with increasing z . The dipole freezing temperature, T_f , can also be determined by analysis of the dielectric loss (ε'') data in the time (frequency) domain. The empirical UDR model allows fitting of a dielectric loss peak as a function of frequency according to:

$$\varepsilon''(f) \propto \frac{1}{(f/f_p)^{-m} + (f/f_p)^{1-n}} \quad (4)$$

where f is the frequency of applied field, f_p is the frequency of the peak maximum and the exponents $-m$ and $1-n$ describe the gradient of the $\varepsilon''(f)$ data below and above f_p , respectively (with the condition that $0 \leq m, n \leq 1$). The UDR theory states the $\varepsilon''(f)$ peak associated with a dipole relaxation should become infinitely broad at dipole freezing, *i.e.*, the exponent m should tend to zero at T_f . Dielectric loss data as a function of frequency for the $z = 0.5$ sample is shown in Figure 8 (a) and indicates that the gradient (m) decreases with decreasing temperature. By extracting the exponent m from this data and extrapolating to $m = 0$ allows an estimation of T_f . The results of such analysis are shown in Figure 8 (b) and summarized in Table 2. The data clearly show a systematic increase in T_f with increasing z (increasing σ^2), and furthermore the values obtained are reassuringly in reasonable agreement with those obtained for the VF fits of the real part of the permittivity when values for the fundamental frequency, f_0 , were constrained to a physically sensible magnitude, Table 2.

In order to look at the self consistency of the results obtained and to highlight the variability in results obtained *via* unconstrained fitting alone, the E_A and T_f values obtained from UDR analysis of the loss data were fed back into the VF model as constrained parameters and the permittivity data fitted once more - the results are collated in Table 2. The most striking result is the consistency in results obtained *via* VF fitting where either f_0 was constrained to a physically sensible limit, or where T_f had been determined from the UDR analysis of the loss data (which has demonstrated to be a robust methodology^{9, 16}); these data show a clear increase in dipole stability (quantified by T_f) with increasing local strain (quantified by variance, σ^2), Figure 9 (a). Both the unconstrained VF fits and those with E_A values obtained from UDR give no consistent

trends in T_f but noticeably both also have f_0 values which cover several orders of magnitude, a result which cannot easily be explained by such minor compositional and structural changes and which in some cases give such high frequencies as to be not physically plausible^{18, 19}. The reasons for these variations are discussed in the next section, however, considering the other results it is apparent that in the so called “fixed cell” samples with invariant average structure but increasing local variations, there is a clear and systematic change in the dielectric response as most simply evident in the displacement of the permittivity-temperature profiles (see ESI). In depth analysis allows this relationship to be quantified in more detail as shown in Figure 9, but it is important to link back to the original (Ba,Sr,Ca) samples which have both varying local and average structures and T_m data for the “fixed cell” samples are included for comparison in Figure 3 (b). This shows a clear relationship between dipole stability and local structural variations in these materials.

Discussion

It is clear that VF fitting of permittivity data should be treated with caution as the parameters obtained are highly sensitive, and often give results which do not vary systematically, or which have a significant spread which cannot easily be explained by minor variations in composition and/or crystal structure. The reasons for these variations are clearly demonstrated by considering how the three fitting parameters (T_f , f_0 , and E_A) relate to the data fits in Figure 6 (a): T_f and f_0 are obtained at the limits when $f \rightarrow 0$ and $f \rightarrow \infty$, *i.e.*, where the extrapolated fit tends to vertical and horizontal, respectively; the curvature of the fit is determined by E_A . Due to the combination of the degree of frequency and temperature dispersion displayed by relaxor materials and also the limited frequency range of most experimental apparatus, the $T_m(f)$ data available for VF fitting are limited to a rather narrow range and the fit is extrapolated over many orders of magnitude as shown by replotting the fits shown in Figure 6 (a) on an extended scale in Figure 10. It becomes obvious therefore that even small variations in $T_m(f)$ data (due *e.g.*, to ceramic microstructure effects) can dramatically effect the parameters obtained. In order to mitigate against this, it is expedient to either place some physically sensible restrictions on one or more parameters (*e.g.*, f_0 – Table 2), or to corroborate them by alternative methods such as fitting the loss data to the UDR model. The latter approach is preferable and allows some self-consistency in the VF parameters to be evaluated. A more robust, and consistent alternative is UDR analysis of the loss data and

determination of T_f by extrapolation of the m exponent of the loss peak in the frequency domain which has been shown to be consistent and relatively insensitive to ceramic microstructure.

The dielectric data show that Sr and/or Ca substitution at the A-site displaces the dielectric curves to higher temperature. The magnitude of this displacement however is not easily reconciled by a simple size effect argument. Instead the temperature dependence of the dipole stability in these relaxor materials appears to be better described by the A-cation size variance, *i.e.*, the degree of size mis-match and combined UDR analysis and restricted VF fits show that the dipole freezing temperature (T_f) varies linearly with size variance (σ^2). The effect of size variance in dipolar oxides was first studied by Sinclair and Attfield¹⁴ in Sr- and Ca-doped BaTiO₃. They demonstrated that while the effect on the Curie temperature, T_C (which represents the dipole stability) could not be readily explained by a simple size (tolerance factor) argument, there was a clear relationship with size variance. They also reported a linear dependence with $dT_C/d\sigma^2$ of 14,500-16,000 KÅ⁻² compared to values of *ca.* 50,000 KÅ⁻² for the structural transition in A₂CuO₄ compounds and *ca.* 20,000 KÅ⁻² for the magnetic transition in AMnO₃ perovskites. They attributed these differences to the differing mechanisms and suggested that *ca.* 15,000 KÅ⁻² was the signature of a displacive (dipolar) transition. A linear fit of T_f (determined from the UDR analysis) *vs.* σ^2 , shown in Figure 9 gives $T_f/d\sigma^2 = 15,800$ KÅ⁻², in excellent agreement with dipolar Ti displacements in ferroelectric Ca-BaTiO₃. This result is perhaps not unsurprising given that the dipolar nature of both systems arises due to B-cation displacements within the oxygen octahedra.

Sinclair and Attfield¹⁴ did not describe the atomistic mechanism of dipole stabilisation, merely surmising that it was likely due to lattice strain. In a later study, Levin *et al.*²⁰ used XAFS to study the local structure in both Ca- and Sr-doped BaTiO₃. Their study showed that while Sr remains centric in the A-site, Ca is displaced and this couples with the neighbouring B-site Ti displacements, stabilising it and sustaining T_C . This work has since been corroborated by the computational work of Dawson *et al.*²¹ In simple crystallo-chemical terms this is rather easily understood: Ca is too small for the large 12-coordinate A-site of a cubic perovskite oxide and hence CaTiO₃ undergoes a distortion to orthorhombic $Pbnm$ symmetry (the GdFeO₃ structure) which involves octahedral tilting to reduce the A-site volume and concomitant “anti-polar” A-site displacements in order to reduce the Ca coordination from 12 to the preferred 8. In our recent

work on RE₂ScO₃ (RE = La, Nd, Gd) doped BaTiO₃ we argued that in a Ba-rich lattice the octahedral tilts are frustrated due to surrounding Ba-containing A-sites resisting this volumetric contraction, and as a result only the A-site displacement mode remains to optimise the preferred bonding environment of the smaller A-site dopant cation²². This A-site displacement couples with the B-site and stabilises T_C .

It is not immediately clear, however, why it is the statistical size variance rather than absolute size dependence (*i.e.* T_C or T_f has a root rather than reciprocal relationship with size). The work by Dawson *et al.*²¹ suggests a delicate balance of A-site and B-site (octahedral) volume contraction and it may be coincidence that variance reflects this balance. In any case it appears that the statistical size variance allows a metric of “local structure” to be determined and which clearly has an effect on the dielectric properties. Such local information is not readily available by traditional diffraction methods and techniques which provide local structural information (such as XAFS or PDF) are required.

Conclusions

The effect of isovalent A-site doping on the dielectric response of a family of relaxor TTBs was investigated using neutron and x-ray diffraction and in-depth analysis of dielectric data. The dielectric analysis showed that fitting of permittivity data to the widely used Vogel-Fulcher model should be treated with caution and that fitting of dielectric loss data according to the Universal Dielectric response model is a more reliable and robust method for determining the dipole freezing temperature, T_f (which is a measure of dipole stability) in these materials.

The crystallography, as determined by neutron and x-ray diffraction, indicated that all compositions obeyed Vegard’s law with unit cell metrics decreasing monotonically with decreasing average A-cation size. In contrast the dipole stability did not vary in a similarly systematic way with A-cation size but instead T_f is directly proportional to the statistical A-cation size variance. The variance provides a measure of local structure and so it is clear that local structure plays a significant role in the dielectric response. Such information is not available *via* conventional Rietveld analysis of diffraction data and probes of local structure are required. Nevertheless, it appears that variance may be a useful metric to guide the tuning of

properties in TTBs and could be extended to other structure types which contain perovskite units such as Ruddlesen-Popper and Dion-Jacobsen phases.

Acknowledgements

The authors would like to acknowledge EaStCHEM and EPSRC (Grant No. EP/F004133/1) for financial support, and Dr Clemens Ritter of the ILL for assistance in collection of neutron diffraction data.

References

1. P. G. Dickens and M. S. Whittingham, *Quarterly Reviews, Chemical Society*, 1968, 22, 30.
2. A. Simon and J. Ravez, *Comptes Rendus Chimie*, 2006, 9, 1268-1276.
3. P. B. Jamieson, S. C. Abrahams and J. L. Bernstein, *J. Chem. Phys.*, 1969, 50, 4352.
4. P. Labbe, H. Leligny, B. Raveau, J. Schneck and J. C. Toledano, *Journal of Physics: Condensed Matter*, 1990, 2, 25-43.
5. P. B. Jamieson, S. C. Abrahams and J. L. Bernstein, *J. Chem. Phys.*, 1968, 48, 5048.
6. I. Levin, M. C. Stennett, G. C. Miles, D. I. Woodward, A. R. West and I. M. Reaney, *Appl Phys Lett*, 2006, 89, 122908.
7. M. C. Stennett, I. M. Reaney, G. C. Miles, A. R. West, C. A. Kirk and I. Levin, *J. Appl. Phys.*, 2007, 101, 104114.
8. D. C. Arnold and F. D. Morrison, *Journal of Materials Chemistry*, 2009, 19, 6485-6488.
9. A. Rotaru, D. C. Arnold, A. Daoud-Aladine and F. D. Morrison, *Physical Review B*, 2011, 83, 184302.
10. A. Rotaru, A. J. Miller, D. C. Arnold and F. D. Morrison, *Philosophical transactions. Series A, Mathematical, physical, and engineering sciences*, 2014, 372, 20120451.
11. J. Gardner and F. D. Morrison, *Dalton transactions*, 2014, 43, 11687-11695.
12. R. D. Shannon, *Acta Crystallographica Section A*, 1976, 32, 751-767.
13. J. P. Attfield, *Chemistry of Materials*, 1998, 10, 3239-3248.
14. D. C. Sinclair and P. J. Attfield, *Chemical Communications*, 1999, 1497-1498.
15. D. Viehland, S. J. Jang, L. E. Cross and M. Wuttig, *J. Appl. Phys.*, 1990, 68, 2916.
16. A. M. Rotaru, F.D. Morrison, *Journal of Thermal Analysis and Calorimetry*, 2015, in press.
17. A. K. Jonscher, *Dielectric Relaxation in solids*, Chelsea Dielectrics Press, London, 1983.
18. F. Bahri, H. Khemakhem, M. Gargouri, A. Simon, R. Von der Mühl and J. Ravez, *Solid State Sci*, 2003, 5, 1445-1450.
19. H. Du, W. Zhou, F. Luo, D. Zhu, S. Qu and Z. Pei, *J Appl Phys*, 2009, 105, 124104.
20. I. Levin, V. Krayzman and J. C. Woicik, *Appl Phys Lett*, 2013, 102, 162906.
21. J. A. Dawson, D. C. Sinclair, J. H. Harding and C. L. Freeman, *Chemistry of Materials*, 2014, 26, 6104-6112.
22. S. Turp, PhD, University of St Andrews, 2013.

Table 1. Unit cell parameters and variance for “fixed cell” compositions with formula $\text{Ba}_4\text{Sr}_{2-z}(\text{Ba}_{0.37}\text{Ca}_{0.63})_z\text{GaNb}_9\text{O}_{30}$.

z	a (Å)	c (Å)	c/a	$\sigma^2 \times 10^3$ (Å ²)
0.5	12.531	3.958	0.316	7.48
1.0	12.533	3.958	0.316	9.26
1.5	12.528	3.956	0.316	10.68
2.0	12.516	3.952	0.316	12.09

Table 2. Calculated values for f_0 , E_A and T_f from the four different Vogel-Fulcher fitting methods employed for $\text{Ba}_4\text{Sr}_{2-z}(\text{Ba}_{0.37}\text{Ca}_{0.63})_z\text{GaNb}_9\text{O}_{30}$ samples.

Method	z	f_0 (Hz)	E_A (eV)	T_f (K)	RMSD	χ^2
Unconstrained	0.5	8.42×10^{11}	0.108	55.1	0.064	0.058
	1.0	4.84×10^{17}	0.404	7.16	0.039	0.021
	1.5	2.41×10^{16}	0.309	50.2	0.040	0.023
	2.0	1.55×10^{16}	0.293	71.0	0.091	0.116
Constrained f_0	0.5	8.42×10^{11}	0.108	55.1	0.064	0.058
	1.0	8.42×10^{11}	0.122	77.9	0.136	0.261
	1.5	8.42×10^{11}	0.116	102	0.122	0.207
	2.0	8.42×10^{11}	0.114	120	0.150	0.315
Constrained T_f	0.5	7.03×10^{11}	0.105	56.0	0.064	0.058
	1.0	4.93×10^{11}	0.114	81.4	0.147	0.302
	1.5	3.17×10^{12}	0.135	96.0	0.102	0.145
	2.0	2.65×10^{11}	0.097	126	0.171	0.408
Constrained E_A	0.5	7.20×10^{10}	0.077	66.8	0.086	0.103
	1.0	2.46×10^{12}	0.139	72.6	0.120	0.200
	1.5	1.36×10^{13}	0.159	88.4	0.082	0.095
	2.0	2.50×10^{15}	0.253	80.2	0.092	0.119

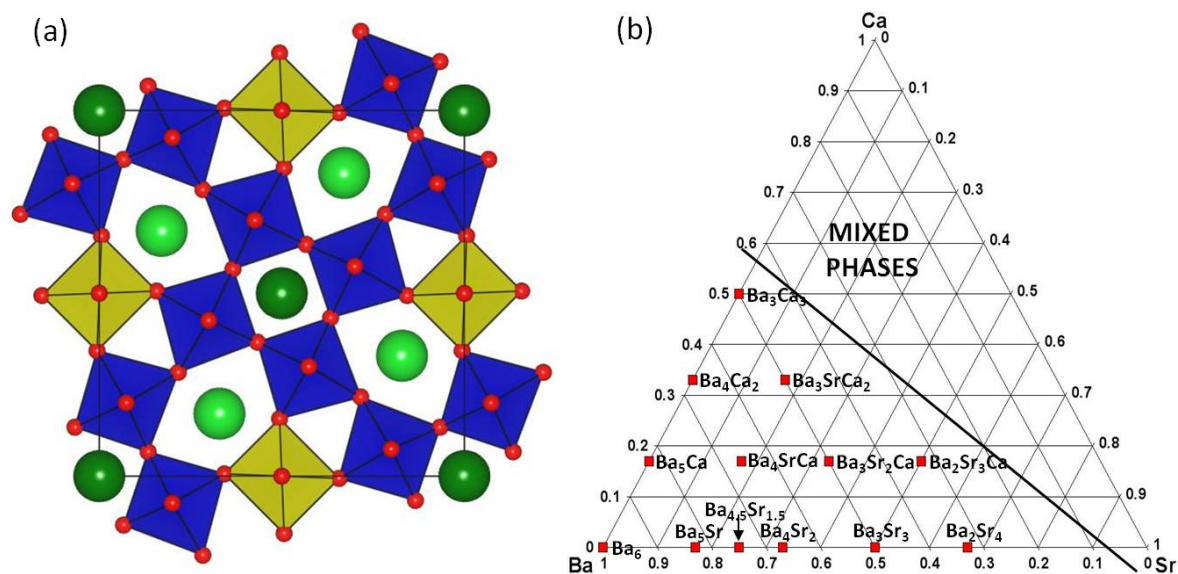


Figure 1. (Colour online). (a) Polyhedral representation of the aristotype $P4/mbm$ tetragonal tungsten bronze (TTB) structure viewed down the c -axis (B1 octahedra are shown in light green, B2 octahedra in dark blue, with A1 and A2 cations represented by dark red and light green spheres, respectively); (b) pseudo-ternary phase diagram showing region of single phase TTB compositions in $Ba_{6-x-y}Sr_xCa_yGaNb_9O_{30}$.

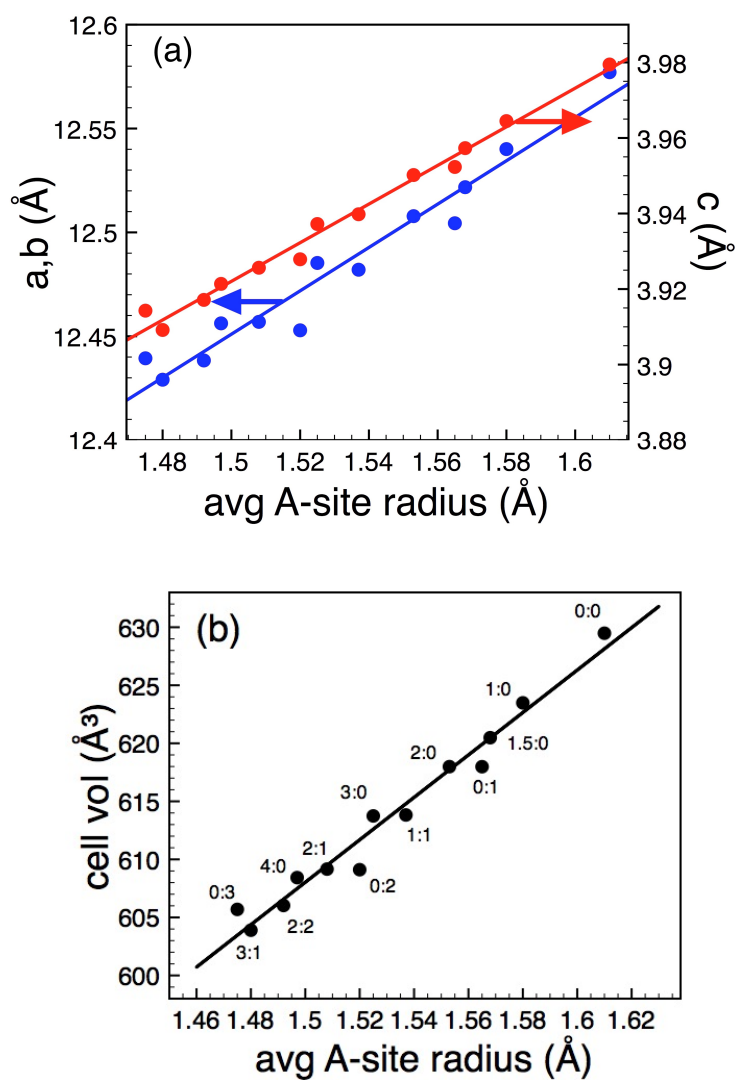


Figure 2. (Colour online). Lattice parameters (a) and unit cell volume (b) as a function of average A-cation size. Compositions are denoted as $x:y$ for $\text{Ba}_{6-x-y}\text{Sr}_x\text{Ca}_y\text{GaNb}_9\text{O}_{30}$. Data obtained from Rietveld refinement of PND data (see ESI for details). Note: error bars are smaller than the symbol size.

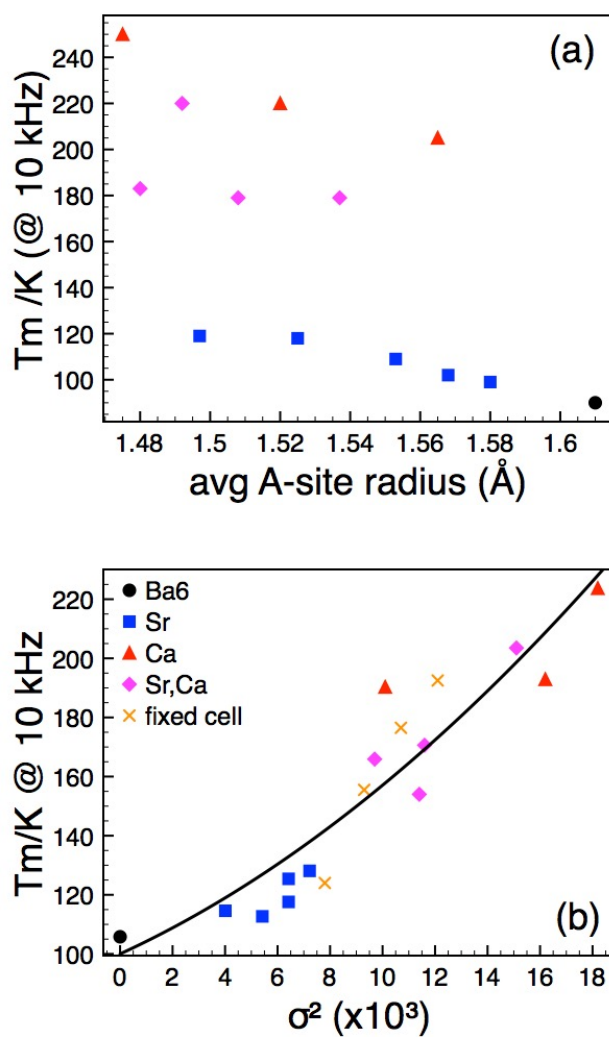


Figure 3. (Colour online). Temperature of permittivity maxima, T_m , (measured at 10 kHz) as a function of (a) average A-cation size, and (b) A-cation size variance, σ^2 .

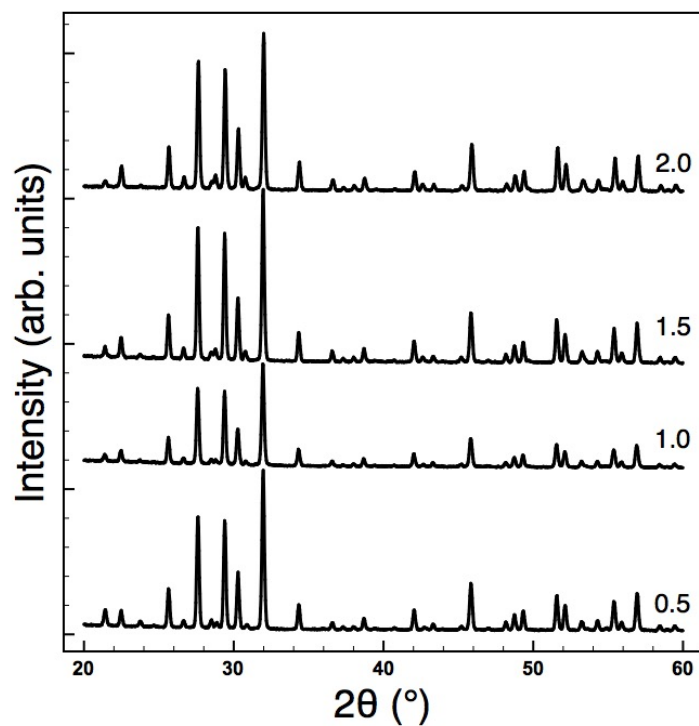


Figure 4. XRD patterns for $\text{Ba}_4\text{Sr}_{2-z}(\text{Ba}_{0.37}\text{Ca}_{0.63})_z\text{GaNb}_9\text{O}_{30}$ compositions, with $z = 0.5, 1.0, 1.5$ and 2.0 , showing invariant lattice parameters (see Table 1).

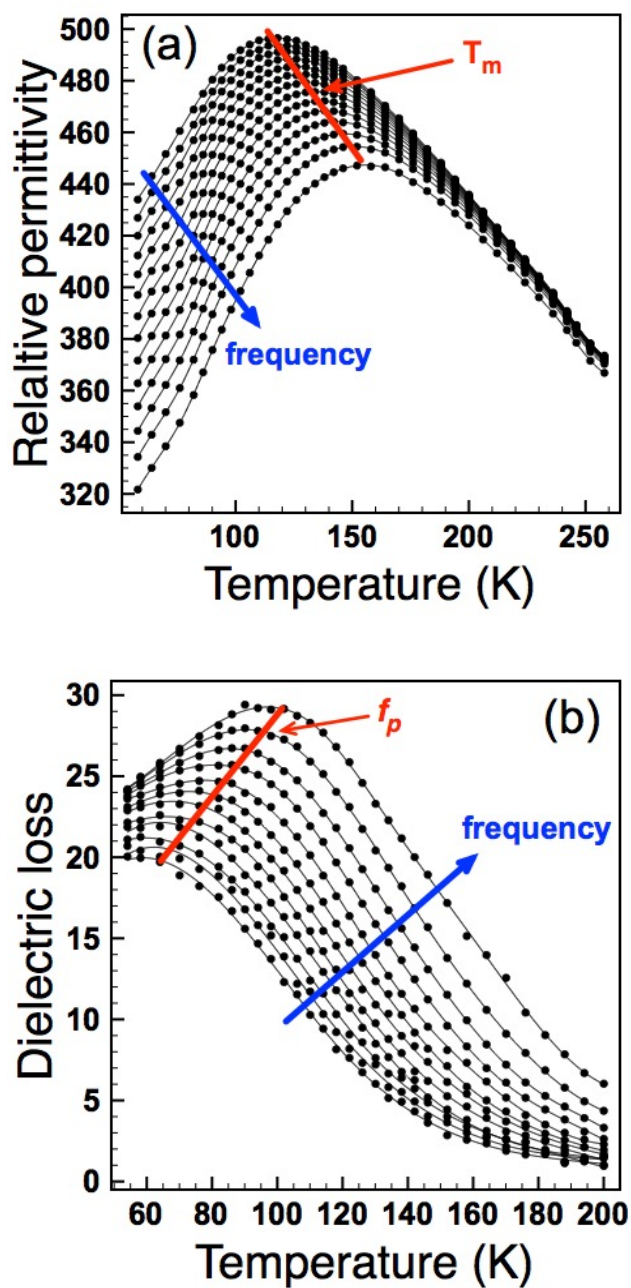


Figure 5. Relative permittivity (a) and dielectric loss (b) as a function of frequency and temperature for $z = 0.5$. Temperature (T_m) and frequency (f_p) maxima used for dielectric analysis are indicated.

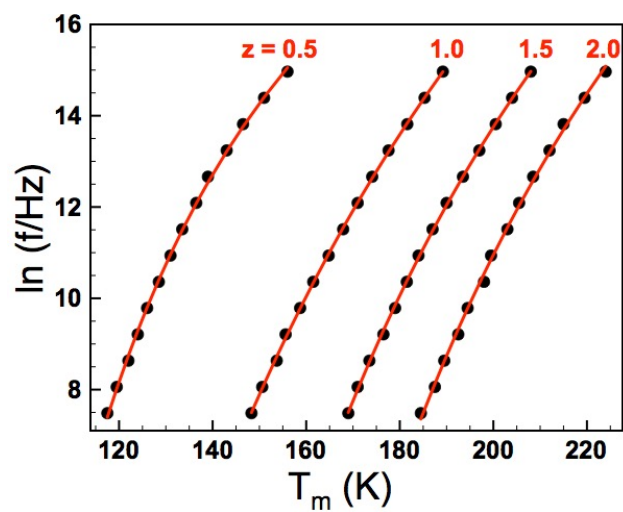


Figure 6. (Colour online) Vogel-Fulcher fits to $T_m(f)$ data obtained from relative permittivity profiles as shown in Figure 5 (a).

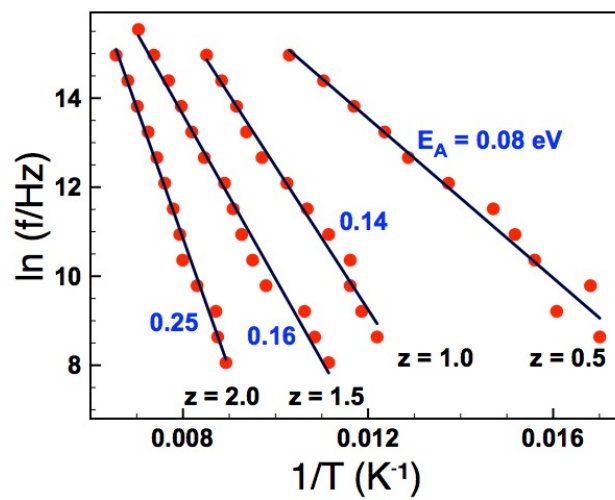


Figure 7. (Colour online) Arrhenius plots of peak frequency (f_p) data obtained from dielectric loss data (as shown in Figure 5 (b)).

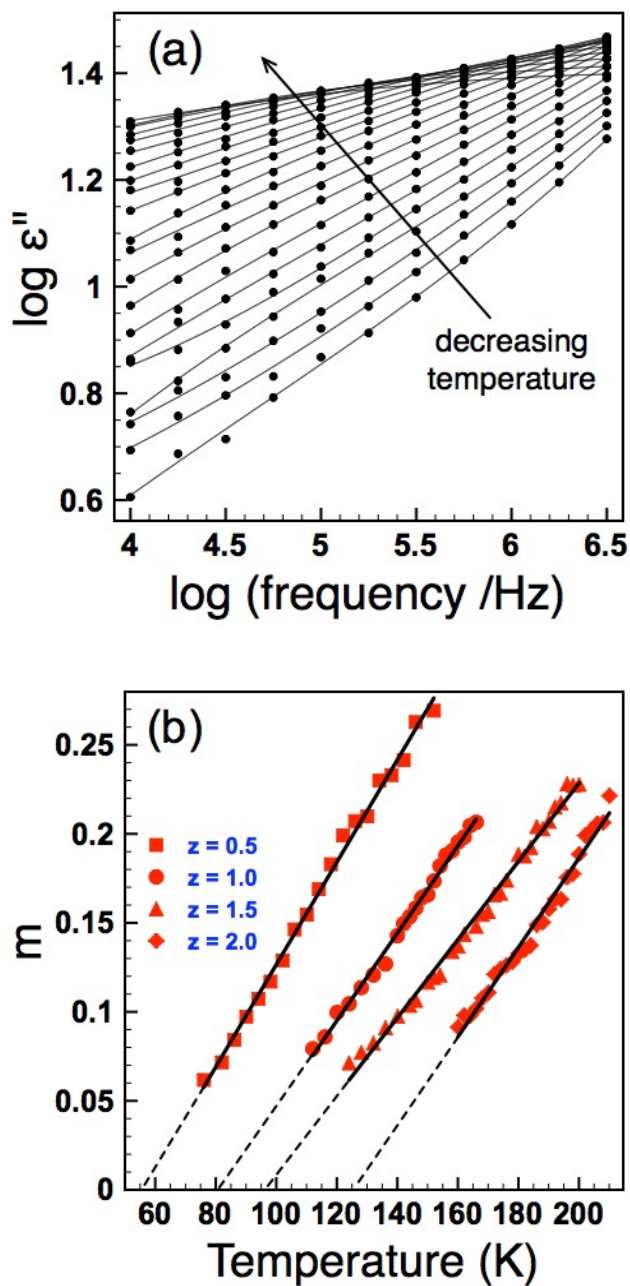


Figure 8. (Colour online) Dielectric loss as a function of frequency showing a decrease in the frequency exponent, m , with decreasing temperature (a); determination of T_f by extrapolation of m to zero (b).

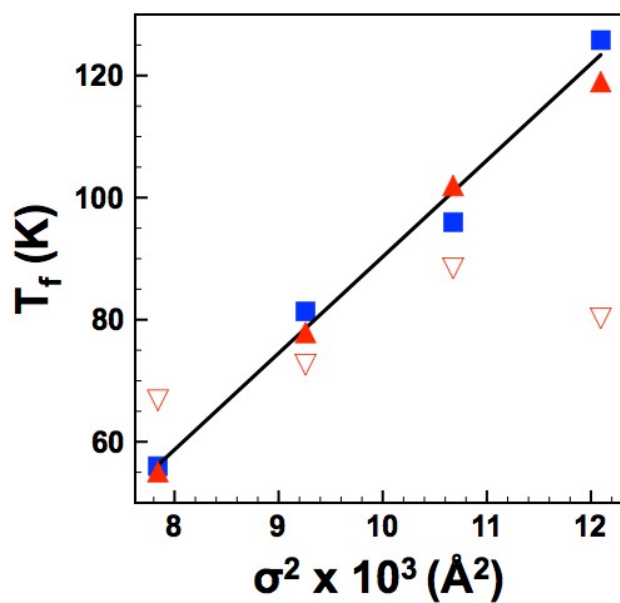


Figure 9. (Colour online) Dipole freezing temperature, T_f , as a function of variance, σ^2 as determined by: UDR analysis (squares); VF fits with constrained f_0 (filled triangles) and constrained E_A (open triangles). Solid line is a linear fit to UDR data.

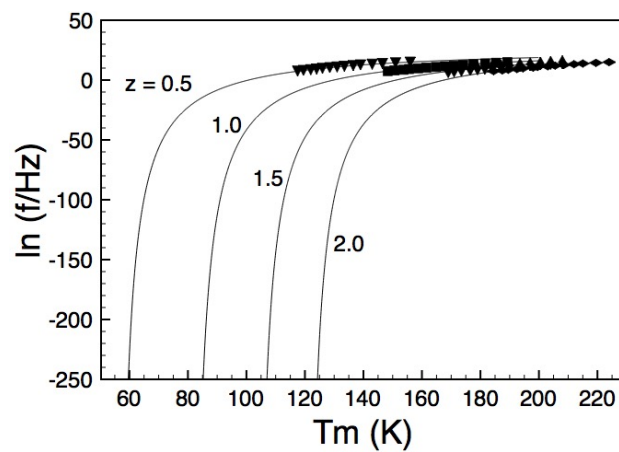


Figure 10. Extended VF fits (with constrained f_0) showing extrapolation for estimation of T_f as $f \rightarrow 0$.